Enhancing environmental models with a new downscaling method for global radiation in complex terrain

Arsène Druel[1], Julien Ruffault[1], Hendrik Davi[1], André Chanzy[2], Olivier Marloie[1], Miquel De Cáceres[3], Albert Olioso[1], Florent Mouillot[4], Christophe François[5], Kamel Soudani[5], and Nicolas K. Martin-StPaul[1].

[1]URFM, INRAE, 84000 Avignon, France
[2]UMR 1114 EMMAH, INRAE, Avignon University, 84000 Avignon, France
[3]CREAF, Centre de Recerca Ecològica i Aplicacions Forestals, Bellaterra, Catalonia, Spain
[4]UMR 5175 CEFE, Montpellier University, CNRS, EPHE, IRD, Montpellier, France
[5]UMR 8079 ESE, UPS, CNRS, AgroParisTech, Orsay, France

Correspondence to: Arsène Druel (arsene.druel@inrae.fr)

Abstract. Global radiation is a key climate input in forest process-based models (PBM) as it determines photosynthesis, transpiration and the canopy energy balance. While radiation is highly variable at fine spatial resolution in complex terrain due to shadowing effects, data required for PBM currently available over large extents are generally at spatial resolution coarser than ~9 km. Downscaling radiation from large-scale to high resolution available from digital elevation models is therefore of potential importance to refine global radiation estimates and improve PBM estimations. In this study, we introduced a new downscaling model that aims to refine sub-daily global radiation data obtained from climate reanalysis or projection at large scales to the resolution of a given digital elevation model. First, downscaling involves splitting radiation into direct and diffuse fraction. Then, the influence of surrounding mountains' shade on direct radiation and the "bowl" (deep valley) effect (or skyview factor) on diffuse radiation is considered. The model was evaluated by comparing simulated and observed radiation at the Mont Ventoux mountain study site (southeast of France) using the recent ERA5-Land hourly data available at 9 km resolution as input and downscaled at different spatial resolution (from 1 km to 30 m resolution) using a digital elevation model. The downscaling algorithm improved the reliability of radiation at the study site in particular at scales below 150 m. Finally, by using two different process based models (CASTANEA, a process-based model simulating tree growth, and SurEau, a plant-hydraulic model simulating hydraulic failure risk), we showed that accounting for fine resolution radiation can have a great impact on predictions of forest functioning.

Short summary. Accurate radiation data are essential for the understanding of ecosystem functioning and dynamics. Traditional large-scale data lack the precision needed for complex terrains. This study introduces a new model to enhance radiation data resolution using elevation maps, which accounts for sub-daily direct and diffuse radiation effects caused by terrain features. Tested on a mountainous area, this method significantly improved radiation estimates, benefiting predictions of forest functioning.

1 Introduction

Studies assessing the impacts of climate change on forest ecosystem functions increasingly rely on high resolution spatial and temporal climate data. For example, process-based models that aim to evaluate the effect of climate on forest functions and services require daily or sub-daily temporal resolution meteorology as input (*e.g.*, Davi et al., 2006; De Cáceres et al., 2023; Granier et al., 2007; Ruffault et al., 2013, 2022, 2023) to simulate key ecophysiological processes (transpiration, photosynthesis or water potential). Yet, even relatively fine-grained (*i.e.*, 1 km) historical or projected climate products (Hijmans et al., 2005; Brun et al., 2022) do not correspond to the "topographic scale" and cannot reproduce fine-scale patterns observed in heterogeneous landscapes. Moreover, employing spatially-coarse climatic projections can lead to biased and irrelevant inferences of local ecological patterns (Bedia et al., 2013) or to substantial errors in impact studies (e.g., Patsiou et al., 2014; Randin et al., 2009). Improving methodologies to provide climatic data at high spatio-temporal resolution variation is therefore crucial to better understand and predict the spatial heterogeneity in forest structure and functions.

Among climate variables, radiation is a key driver of plant functioning and productivity globally (Churkina and Running, 1998), acting through two main mechanisms. On one hand, global radiation determines the photosynthetically active radiation (PAR), *i.e.*, the available energy for photosynthesis and thus plant productivity. Numerous studies have shown the relationship between the amount of solar radiation and the distribution of plant species or communities worldwide (Dirnbock et al., 2003; Franklin, 1998; Meentemeyer et al., 2001; Tappeiner et al., 1998; Zimmermann and Kienast, 1999). On the other hand, the radiation reaching a vegetation surface is an important component of the canopy energy balance, driving surface temperature and vapour pressure deficit (Monteith, 1981). Radiation is thus a key driver of evapotranspiration which enters in most potential evapotranspiration formulations (Fisher et al., 2011) and water balance models (Granier 1999; Ruffault et al. 2013; De Cáceres et al., 2015). Through its effect on leaf temperature and vapour pressure deficit, radiation also influences the water status of the leaves which in turn will drive many plant functions including growth, stomatal aperture and desiccation (Martin-StPaul et al., 2023).

In regions with a complex orography, climatic variations can occur over distances ranging from a few metres to a few kilometres. This phenomenon, referred to as topoclimate (Bramer et al., 2018), can play a crucial role in shaping flora and fauna habitat as well as a multitude of ecosystem processes related to climatic variability (Austin, 2002; Piedallu & Gégout, 2008; Randin et al., 2009). Accounting for topographic effects on spatial radiation patterns has been well studied with the purpose, for instance, of improving niche models (that predict the distribution of plants as a function of environmental variables) in mountainous areas (Piedallu & Gégout, 2008; Randin et al., 2009). So far, such radiation data are measured or computed from local meteorological stations, from coarse-scale global meteorological products such as reanalyses, or geostationary satellite data products at few kilometer resolution (e.g. De Cáceres et al., 2018, Roerink et al. 2012).

Direct radiation is a primary driver of topoclimate variations, as it can undergo changes at a very local scale due to several processes. At the scale of a massif, the surrounding topography can cast shadows on a given point because the sun rays can be physically interrupted. In other words, the presence of nearby high peaks will impact the rays directly coming from the sun. At the scale of a point in space, the slope and aspect (azimuth), will in addition modify the direct radiation intensity received. In the northern hemisphere, a south face will receive more radiation than a north face, and this will be modulated by the angle between the sun rays and the slope at the point. Similarly, the surrounding topography will affect diffuse radiation (*e.g.*, on cloudy days) isotropically (at 360°), leading to lower radiation in valley bottoms (*i.e.*, the skyview factor or the "bowl effect").

Historically, the primary method for accounting for the effects of topography on radiation has been to rely on slope or aspect. Indeed, these parameters are relatively simple to measure (e.g., through GIS) and the global radiation flux at the surface can be easily derived from those (Austin et al., 1990; Carroll et al., 1999; Clark et al., 1999; Pierce et al., 2005). However, this downscaling approach overlooks a significant portion of the processes involved in radiation attenuation due to sky obstruction by surrounding topography. Shading and the skyview were taken into account at a later stage, in particular in the radiation parameterization scheme (Müller & Scherer, 2005) and in several of its applications (e.g. Senkova et al., 2007; Buzzi, 2008). Regional climate models (RCMs), on the other hand, calculate radiation by accounting for atmospheric processes in relation to land-surface processes (energy balance etc…). Nevertheless, they typically operate on fixed grids, usually at scales of several kilometres (Bailey et al., 2023), which is not precise enough for operational use at point level. More recently, another method employed is statistical downscaling, which is empirical and based on regressions (Davy & Kusch, 2021; Fealy & Sweeney, 2008) or machine learning techniques (Hernanz et al., 2023). However, this requires a lot of field data in different contexts to elaborate an empirical model.

Piedallu & Gégout (2008) proposed one method using the slope and the aspect of the point to compute the sun intensity and taking into account the surrounding topography to compute radiation accounting for direct shadowing. They produced a fine scale map (50 * 50 m) over France which is dedicated to statistical niche modelling or mortality risk assessment (Piedallu & Gégout, 2008). However, in the case of process-based vegetation models this has several limitations. Firstly, their approach relies on interpolated meteorological station data to compute the radiation correction at a monthly time step and is thus limited in terms of temporal and spatial accuracy, leading to significant biases in vegetation growth or the smoothing of climatic extremes. Secondly, they do not separate diffuse and direct radiation using clouds but only use an empirical correction of the total radiation using cloud cover. Finally, the skyview factor on diffuse radiation is not taken into account. This method based on measurements is thus limited for projection purposes and requires a large network of equipped stations, resulting in uncertainty. Moreover, it has been applied only to France and has not been generalised to other regions or periods.

In this study we present a process-based method to downscale coarse resolution (0.1° at best in general for reanalysis or meteorological models) or geostationary products (2 km resolution at best) global radiation data (such as global reanalysis or climate projections) made on flat surfaces down to the level of 1 km to 30 m resolution Digital Elevation Model (DEM) by accounting for slope, aspect,the shadowing effect on direct radiation and for the skyview factor on diffuse radiation. The method can be applied at any resolution, depending on the choice of the DEM. Moreover, it can be applied to any type of radiation data, making it applicable to any region in the world and to historical periods as well as future projections. The possibility to use reanalyses-derived radiation further ensures physical consistency between the different climate variables used in process-based models. The algorithm was tested on Mont Ventoux and compared with PAR measurements recorded during 2 years at 7 sites on this complex topographic area. Finally we evaluated how this new radiation product can impact ecological predictions by simulating the gross primary productivity (GPP) and the risk of drought-induced mortality for the European beech (*Fagus sylvatica)* using two process-based models.

2 Methods

2.1 Radiation downscaling model

The proposed radiation downscaling model aims to refine sub-daily global radiation data obtained from reanalysis at large scales to the resolution of a given DEM. This process-based method can be adapted depending on the input dataset and accounts for the shadowing effect on direct radiation and the skyview factor on diffuse radiation. In order to ensure its versatility and applicability, we reduced the need for external data that can be challenging to obtain at the local scale, such as cloudiness (Dubayah and Loechel, 1997; Piedallu and Gégout, 2007). The only required input is a DEM whose resolution will determine the final spatial resolution of the radiation data.

Our methodology involves four distinct steps, outlined as follows (see Fig. 1 for visualisation):

i. Splitting direct and diffuse radiation from a large-scale global radiation dataset (optional if the data already contain direct and diffuse radiation).

ii. Downscaling direct radiation by considering local topography and shadowing effects.

iii. Downscaling diffuse radiation by estimating the proportion of diffuse radiation that reaches the target point relative to the surrounding topography.

iv. Summing the downscaled direct and diffuse radiation components.

These steps are described in detail in the subsequent sections.

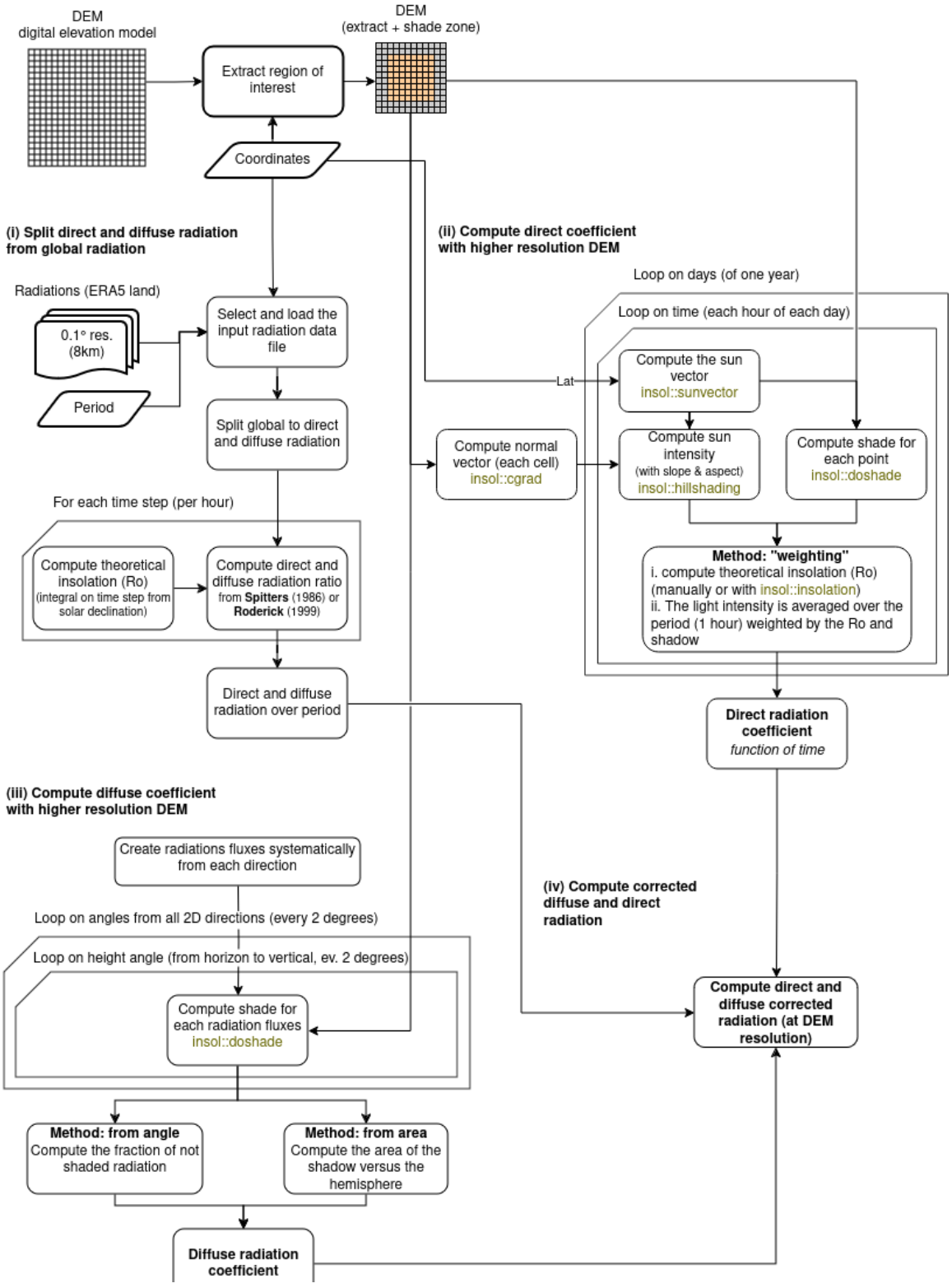
DEM
digital elevation model
Extract region of interest
DEM
(extract + shade zone)
Coordinates
(i) Split direct and diffuse radiation from global radiation
Radiations (ERA5 land)
0.1° res. (8km)
Period
Select and load the input radiation data file
Split global to direct and diffuse radiation
For each time step (per hour)
Compute theoretical insolation (Ro)
(integral on time step from solar declination)
Compute direct and diffuse radiation ratio from Spitters (1986) or Roderick (1999)
Direct and diffuse radiation over period
(ii) Compute direct coefficient with higher resolution DEM
Loop on days (of one year)
Loop on time (each hour of each day)
Lat
Compute the sun vector
insol::sunvector
Compute normal vector (each cell)
insol::cgrad
Compute sun intensity
(with slope & aspect)
insol::hillshading
Compute shade for each point
insol::doshade
Method: "weighting"
i. compute theoretical insolation (Ro) (manually or with insol::insolation)
ii. The light intensity is averaged over the period (1 hour) weighted by the Ro and shadow
Direct radiation coefficient
function of time
(iii) Compute diffuse coefficient with higher resolution DEM
Create radiations fluxes systematically from each direction
Loop on angles from all 2D directions (every 2 degrees)
Loop on height angle (from horizon to vertical, ev. 2 degrees)
Compute shade for each radiation fluxes
insol::doshade
Method: from angle
Compute the fraction of not shaded radiation
Method: from area
Compute the area of the shadow versus the hemisphere
Diffuse radiation coefficient
(iv) Compute corrected diffuse and direct radiation
Compute direct and diffuse corrected radiation (at DEM resolution)

Figure 1: Simplified workflow of radiation downscaling, showing the four different steps of the procedure. The bold boxes at the top left show the data required as inputs (DEM, coordinates, period and large scale radiation), the green boxes show the functions of the external R package used (insol), the truncated boxes show the loops and the rounded boxes show the various stages.

2.1.1 Splitting direct and diffuse radiation

In cases where only global radiation is available from the input dataset, as in products like ERA5-Land (Muñoz-Sabater et al., 2021), a first step involves extracting hourly direct and diffuse radiation (Fig. 1.i). Various methods exist for this purpose (Oliphant & Stoy, 2018). In this study, we adopted the approach proposed by Spitters et al. (1986). This choice was driven by the relative simplicity of this approach and the fact that it was originally developed for European landscapes. Additionally, we explored other methods, such as the one proposed by Roderick (1999) and the one proposed by Bird and Hulstrom (1981). Results obtained using the Roderick (1999) method align consistently with those presented herein (results not displayed). Unlike the method by Spitters et al. (1986), the method by Bird and Hulstrom (1981) does not rely on global radiation values but instead aims to derive the values of direct and diffuse radiation from theoretical radiation, temperature, humidity, among other factors. However, the outcomes generated by this model significantly deviated from those obtained using the Spitters et al. (1986) method and exhibited inconsistency with available measurements (not shown).

The method of Spitters et al. (1986) that was used in this study is an empirical computation technique based on the ratio between theoretical extraterrestrial irradiance (R_0) and the observed value of global radiation (R_g). Specifically, it operates on the assumption that as the ratio of R_g to R_0 decreases, the proportion of diffuse radiation (R_{diff}) relative to direct radiation (R_{dir}) increases - an effect attributed to cloud cover.

To compute R_0 (in W.m^{-2}), a common physically-based approach involves using the radiation incident on a plane parallel to the Earth's surface and the sine of solar elevation (which is dependent on latitude and solar time), as follows (Spitters et al., 1986; Widén & Munkhammar, 2019):

$$R_0 = R_{sc}\left[1+0.033\times\cos\left(doy\times 360/365\right)\right]\times\sin\left(\beta\right)$$
$$\sin\left(\beta\right)=\sin\left(\lambda\right)\times\sin\left(\delta\right)+\cos\left(\lambda\right)\times\cos\left(\delta\right)\times\cos\left(15\times\left(t_h-12\right)\right) \quad (1)$$
$$\delta=\frac{\pi\times 23.45}{180}\times\sin\left(2\times\pi\times\frac{doy+284}{365}\right)$$

With R_{sc} representing the solar constant (1 361 W.m^{-2}, Coddington et al., 2016), *doy* the day of the year, $\sin\left(\beta\right)$ the sine of the solar elevation angle, λ the latitude of the site (in radian), δ the solar declination angle (in degrees) and t_h the hour (in solar time).

It's important to note that in this study, global radiation is not treated as a singular value but rather as an average over a short period of time (e.g., between h_t and h_{t+1}, using an hourly time step with ERA5-Land). Thus, $\sin\left(\beta\right)$ needs to be integrated:

$$\int_{h_t}^{h_{t+1}} \sin(\beta) = \sin(\lambda) \times \sin(\delta) + \cos(\lambda) \times \cos(\delta) \times \frac{15 \times \pi}{180} \times \left[\sin\left(\frac{\pi}{180} \times 15 \times (h_{t+1} - 12) \right) - \sin\left(\frac{\pi}{180} \times 15 \times (h_t - 12) \right) \right] \quad (2)$$

Then, we used the relationship between the fraction of diffuse radiation (R_{diff}) compared to global radiation data (R_g) and the fraction of global radiation data (R_g) compared to theoretical radiation (R_0), as recommended by de Jon (1980) for hourly radiation (described in Spitters et al., 1986, including values for daily radiation):

$$\begin{aligned}
&\frac{R_{diff}}{R_g} = 1 && \text{for} && \frac{R_g}{R_0} \le 0.22 \\
&\frac{R_{diff}}{R_g} = 1 - 6.4 \times \left(\frac{R_g}{R_0} - 0.22 \right)^2 && \text{for} && 0.22 < \frac{R_g}{R_0} \le 0.35 \\
&\frac{R_{diff}}{R_g} = 1.47 - 1.66 \times \frac{R_g}{R_0} && \text{for} && 0.35 < \frac{R_g}{R_0} \le K \\
&\frac{R_{diff}}{R_g} = L && \text{for} && K < \frac{R_g}{R_0}
\end{aligned} \quad (3)$$

With $L = 0.847 - 1.61 \times \sin(\beta) + 1.04 \times \sin^2(\beta)$ and $K = \frac{1.47 - L}{1.66}$.

Following Spitters et al. (1986), the final step involves subtracting the circumsolar component (R_{circum}) of diffuse radiation from the direct flux: Under clear skies, diffuse irradiance is anisotropic, due to the presence of aerosols in the atmosphere, and the intensity is therefore higher in the direction of the sun. It is thus necessary to attribute the excess diffuse irradiance observed near the direction of global radiation to direct radiation.

$$R_{circum} = \cos^2\left(\frac{\pi}{2} - \beta \right) \times \cos^3(\beta) \quad (4)$$

To determine the corresponding fraction of diffuse radiation under intermediate sky conditions, clear to cloudy skies, we adopt the interpolation method introduced by Klucher (1978):

$$\frac{R_{diff}}{R_g} = \frac{R_{diff}}{R_g} \div \left[1 + \left(1 - \left(\frac{R_{diff}}{R_g} \right)^2 \right) \times R_{circum} \right] \quad (5)$$

Finally, considering that global radiation (R_g) comprises the sum of diffuse (R_{diff}) and direct (R_{dir}) radiation components, the value of R_{dir} can be directly inferred from the other two components.

2.1.2 Downscaling direct radiation

To downscale direct radiation (Fig. 1.ii.), two distinct processes were considered. Firstly, the path of sun rays was examined to determine if any obstruction in the topography may block them. Secondly, if unobstructed, the slope and aspect of the pixel are used to compute the radiation intensity relative to a horizontal surface.

For both processes, the initial step involved computing the sun vector in three dimensions. This was achieved using the R package "insol" (version 1.2.2, Corripio, 2020) and specifically the "sunvector" function, which defines the vector based on longitude, latitude, and time (day, hour, minute). To assess whether radiation is obstructed by a summit, the close topography derived from a DEM is computed using the "doshade" function within the "insol" package. To determine sun intensity, the "hillshading" function from the same package is utilised, requiring both the sun vector and the topography (previously normalised into unit vectors using the "cgrad" function). Note that the same package is now available for python (on https://pypi.org/project/insolation/ and https://www.meteoexploration.com/insol/).

Considering that the input radiation is accumulated over a specific period (e.g., 1 hour in ERA5-Land), and to account for spatial variations in radiation intensity (primarily due to the angle of the sun rays) and shadow projections, several time steps are employed for downscaling the direct radiation. In this study, the default value of three time steps per hour ($n = 3$) was adopted. Additionally, to aggregate the values while considering temporal variations in radiation intensity, each value is weighted by the theoretical extraterrestrial irradiance (R_0 in Eq. (1)). This yields a corrected direct radiation (R_{dir_cor}):

$$R_{dir_{cor}} = R_{dir} \times \frac{\sum_{t_1}^{t_n} \left(R_0 \times S \times \frac{I_{slope}}{I_{vert}} \right)}{\sum_{t_1}^{t_n} R_0} \quad (6)$$

Where S represents the shadow parameter (with a value of 0 indicating shadow and 1 indicating no shadow), and I_{slope} and I_{vert} denote the illumination intensity over the slope and a vertical surface, respectively, to derive the relative intensity of sunlight over the slope.

2.1.3 Downscaling diffuse radiation

Diffuse radiation is independent of the sun's inclination. It emanates uniformly from all directions within the skydome, limited in this study to the top half-sphere. Therefore, its downscaling (Fig. 1.iii) relies on the surrounding topography in all 360° horizontal directions, particularly the proportion of diffuse radiation from all directions that can reach the point under study.

Various methods exist to compute this fraction, including employing numerous random rays or determining, for regular 3D distributed vectors, the level of shadow. In this study, a specific method was devised. It involves computing, for each

azimuth angle (with fixed steps of 2°), the minimum unshaded radiation using the "doshade" R function described previously and a DEM.

Subsequently, these values are utilised to calculate the shaded area of the top half-sphere and thus the proportion of diffuse radiation reaching the focal point. Finally, this proportion is applied to the diffuse radiation computed in Sect. 2.1.1 to derive the corrected diffuse radiation (R_{diff_cor}).

The corrected diffuse and direct radiation can then be directly employed or recombined into corrected global radiation (R_{g_corr}), e.g., to serve as input to a model of forest function or dynamics.

2.1.4 Digital elevation model data

In various steps of the radiation downscaling, the utilisation of a DEM is imperative (Sect. 2.1.2 and 2.1.3). In this study, we evaluated radiation downscaling using different DEMs characterised by varying resolutions.

The first dataset is the DEM provided by the Shuttle Radar Topography Mission (SRTM, 2013), offering a resolution of 1 arc-second (approximately 30 m). In order to clarify the impact of using different resolutions, the resolution of the SRTM product was downgraded to obtain products with resolutions of 60, 90, 125, 185, 250 and 500 metres using the aggregate function (R, terra 1.7.23 library).

An additional series of DEMs was employed: the Global Multi-resolution Terrain Elevation Data 2010 (GMTED2010, Danielson and Gesch, 2011), which encompasses spatial resolutions of 30, 15, and 7.5 arc-seconds, corresponding approximately to resolutions of 1 km, 500 m, and 250 m, respectively. These datasets were compiled from diverse sources. However, for the metropolitan France region, the primary source of the dataset was the 1 arc-second SRTM DEM.

The interest of these DEMs lies in their applicability beyond the geographic scope covered in this study. Their availability at a global terrestrial scale renders them suitable for use in various locations worldwide (with the exception of SRTM, which is limited to latitudes between 60° north and 56° south).

2.2 Study area

The study area was Mont Ventoux, a mountain located in southeastern France, with its highest point reaching an elevation of 1912 metres (44.174° N - 5.27794° E) (Fig. 2). While Mont Ventoux is predominantly oriented in an east-west direction, it exhibits notable variations in slopes and aspects. The southern flank is characterised by gradual inclines, whereas steeper slopes are evident on its northern side. Mont Ventoux presents a predominantly wooded landscape, featuring a mixed beech-fir forest on its northern side, and a mixed European beech-black pine forest on its southern side, particularly above an elevation of 800 metres (Jean et al., 2023). Below this elevation, the dominant species are more typical of the Mediterranean biome and include coppices of downy oak (*Quercus pubescens*), evergreen oak (*Quercus ilex*), Aleppo pine (*Pinus halepensis*) as well as as natural regeneration of Atlas cedar (*Cedrus atlantica*) from old plantation trials of the early 20th century.

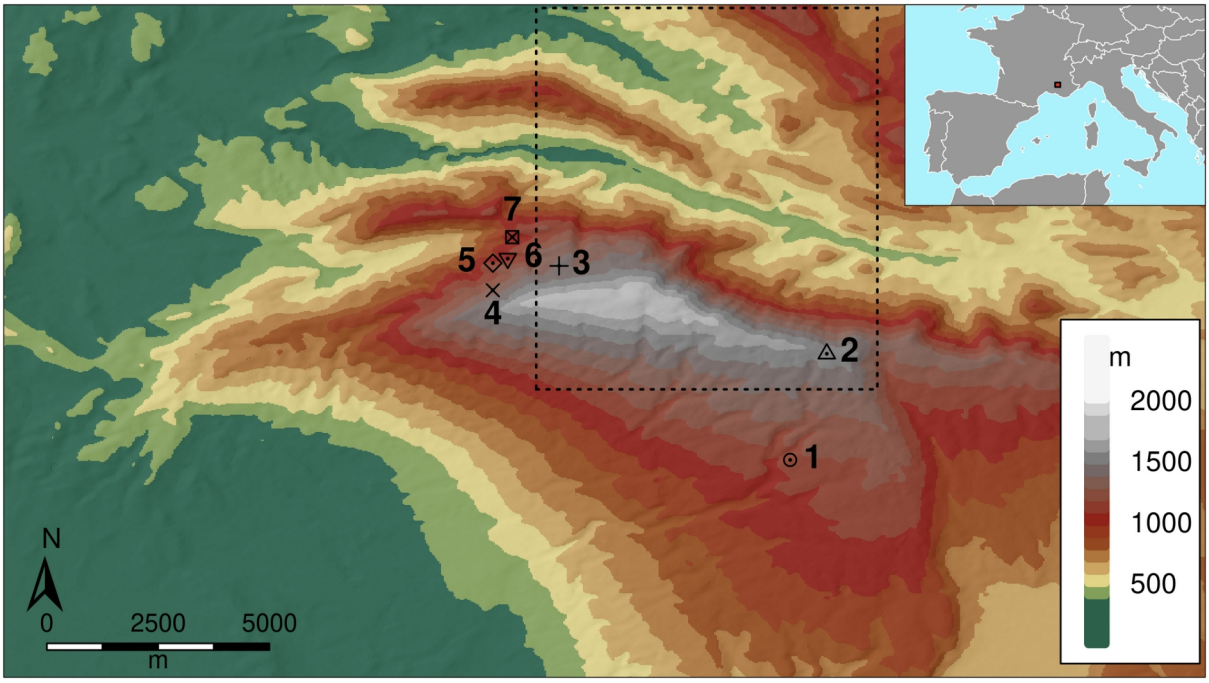

Figure 2: Map of the study area (Mont Ventoux). Mont Ventoux is located in southeastern France (see in the inset). Observation points (one symbol with associated number) and the ERA5-Land tile (in dotted line) used in this study are indicated.

2.3 Global radiation measurements

On June, 27 2016, we installed seven mini-weather stations at different strategic elevations and locations on Mont Ventoux (Table 1), each equipped with loggers (YBdesign) and sensors for photosynthetically active radiation (PAR, 400-700 nm), temperature and relative humidity. The sensors were installed on a vertical pole and positioned horizontally (levelled with a spirit level). The PAR sensors (CBE80, brand Solems) and the thermo-hydrometers (EE07-PFT, brand E+E) were calibrated using a reference weather station at the INRAE campus of Avignon before the beginning of the experiment. The mini-weather stations were positioned in clearings with forest edges extending at a distance minimum of 30 m from the station. The data were recorded at one hour timestep. The photosynthetic flux density delivered by the sensors were converted into $W.m^{-2}$ of global radiation using an empirical relationship calibrated on the ICOS Font-Blanche experimental site (Moreno et al., 2021).

N°	Site	Latitude (°)	Longitude (°)	Elevation (m)	Slope (°)	Aspect(°)
1	Les Tournières	44.129646	5.320524	1159	5.5	250.1
2	Col de la fache	44.157819	5.331975	1575	6.2	201.2
3	Mont Serein	44.182886	5.257725	1413	4.0	234.1

4	dvx5	44.176758	5.238861	1320	20.8	347.2
5	Tc2	44.184014	5.239161	1116	33.1	351.0
6	dvx2	44.185142	5.243383	1074	28.0	355.1
7	142	44.190856	5.244869	1050	23.0	188.4

Table 1. List and main characteristics of the observation sites in Mont Ventoux where radiation measurements were performed. Slope and aspect (azimuth) was computed from a 30 m resolution SRTM digital elevation model.

The observed radiation was compared with the radiation from ERA5-Land before and after downscaling using DEMs at different resolutions. In order to facilitate the comparison between the ERA5-Land reanalysis dataset and observations, which may contain some gaps due to power failure, we aggregated radiation data over various periods (annually or seasonally). This approach involved excluding time steps with missing data, separately for each site. Moreover, to compare with these observations, the correction of the light intensity due to the angle of the direct light rays in relation to the slope and aspect (Sect. 2.1.2, the 'hillshading' function) was deactivated (in Sect. 3.1), as the measurements were carried out on a device placed horizontally.

2.4 Modelling the effect of radiation downscaling on plant functions

To quantify the influence of downscaled radiation on specific applications, we assessed the impact of radiation downscaling on beech (*Fagus sylvatica*) forest functioning using process-based vegetation modelling on the mountainous area of the Mont Ventoux massif (where radiation measurements were located).

We employed two complementary forest vegetation models to quantify how radiation downscaling affects the spatial patterns of both Gross Primary Productivity (GPP) and drought-induced risk of hydraulic failure. These models are, respectively, the forest growth model CASTANEA (Dufrêne et al., 2005) and the plant hydraulic model SurEau (Cochard et al., 2021; Ruffault et al., 2022).

CASTANEA is a comprehensive forest soil-vegetation-atmosphere model coupled with a growth module. It simulates carbon (photosynthesis and respiration) and water fluxes (transpiration, soil water content, soil water potential) at a half-hourly to daily time step for an average tree in a homogeneous forest stand. A carbon allocation module assigns a proportion of the daily Net Primary Productivity (NPP) toward various plant compartments (stem, roots, fine roots, flowers, acorn, leaves, and storage) using empirical coefficients. Carbon and water fluxes, including gross and net ecosystem photosynthesis, respiration, transpiration, latent heat fluxes, soil water content, and plant water potential, have been validated on different species and sites, including beech on Mont Ventoux (Davi et al., 2005; Cailleret et al., 2011; Delpierre et al., 2012). In this study, the canopy Gross Primary Productivity (GPP) was used to demonstrate the effects of radiation downscaling on potential productivity.

SurEau is a plant-hydraulic model that is dedicated to simulate the risk of drought-induced hydraulic failure due to xylem embolism, a leading mechanism of plant mortality under drought (Cochard et al 2021; Ruffault et al 2022). The model simulates water fluxes and water potential along the soil-plant hydraulic continuum at a half hourly time step, and considers leaf stomata and its regulation, and cuticular transpiration plant organ capacitance an. The model is parameterized with various measurable plant traits previously collected for the target species (Ruffault et al., 2022). In this study, drought-induced risk of hydraulic failure (or the percentage loss of hydraulic conductance) in the vascular system was used as a proxy for hydraulic risk during a given summer.

We conducted spatial simulations for one pixel at 0.1° resolution (~ 11 km * 8 km at these coordinates), covering a large part of the Mont Ventoux northern face where the measurements were conducted. The simulations covered the years 2016 and 2017, encompassing the same geographical area as outlined in Sect. 2.3, spanning a segment of Mont Ventoux ranging from 5.25° W to 5.35° W and from 44.15° N to 44.25° N.

Climate data were directly sourced from the ERA5-Land hourly dataset (Muñoz-Sabater et al., 2021), including temperature, precipitation, wind speed, relative humidity, and global radiation. The latter was downscaled using the method presented in Sect. 2.1, employing one of the DEMs discussed in Sect. 2.1.4.

To maintain consistency and avoid introducing uncertainty from disparate datasets, all other non-climatic inputs were set constant across the study area, as described hereafter. The species selected, *Fagus sylvatica* (European beech), is one of the most common species present on Mont Ventoux (Lander et al., 2021) and its traits are already available for the two models (Cailleret & Davi, 2011; Cailleret et al., 2013; Davi & Cailleret, 2017; Ruffault et al., 2022), with a Leaf Area Index set at 3.5. The soil characteristic corresponded to the median value extracted from the whole studied area from the SoilGrids database (Poggio et al., 2021).

3 Results

3.1 Comparison between simulated and observed global radiation

The comparison of ERA5-Land global radiation, both uncorrected and corrected, with observed global radiation across the 7 studied sites showed the benefit of our downscaling method in accurately estimating local global radiation (Figs. 3, 4 and Table 2).

Specifically, the correlation between observed and simulated yearly mean global radiation increased from $r^2 = 0.59$ to $r^2 = 0.93$, while the RMSE decreased from 33.5 to 8.6 $W.m^{-2}$, for the raw ERA5-Land radiation and ERA5-Land radiation corrected with a 30 m resolution DEM, respectively (Fig. 3 and Table 2). However, this increase in the performance of estimating global radiation did not progress consistently as the resolution of our downscaling approach increases. We

observed a slight and heterogeneous improvement in the corrected radiation from 1 km to 250 m resolution compared to the raw ERA5-Land resolution (around 9 km). It is not until the resolution reaches around 200 metres that a significant and continuous improvement was observed (decrease in RMSE, increase in r^2) until 30 m resolution (Fig. 4).

Our results further showed that the absolute performance of radiation models (in terms of r^2) and their relative differences remained consistent across the different studied seasons (Table 2), despite some particularities. During winter, ERA5-Land raw data showed weak correlation with observations (r^2 at 0.37 and RMSE at 38 $W.m^{-2}$), which substantially improved with correction (r^2 = 0.90, RMSE = 11 $W.m^{-2}$). Similarly, but more pronounced, in autumn correlations and RMSE were considerably enhanced (respectively r^2 from 0.21 to 0.94 and RMSE from 45 to 9 $W.m^{-2}$). In summer, the correlation was almost zero with the ERA5-Land data, whereas it exceeded 0.5 with the corrected radiations. In contrast, the correlation was stable and high (0.85) in spring but did not improve with downscaling, while RMSE improved with correction (35 to 23 $W.m^{-2}$). Further analysis also revealed that the uncorrected (Fig. 3.a) and corrected (Fig. 3.b) seasonal data showed different behavior and so the equations of the seasonal curves for corrected ERA5-Land radiation closely aligned with the 1/1 line, in accordance with an important decrease in RMSE. It is noteworthy that most of the improvement came from points located on northern slopes (points 4, 5 and 6, Fig. 3). Accordingly, the daily bias from those points was reduced compared to uncorrected data, while points located on flat surfaces or southern slopes showed low and not significant bias (not shown).

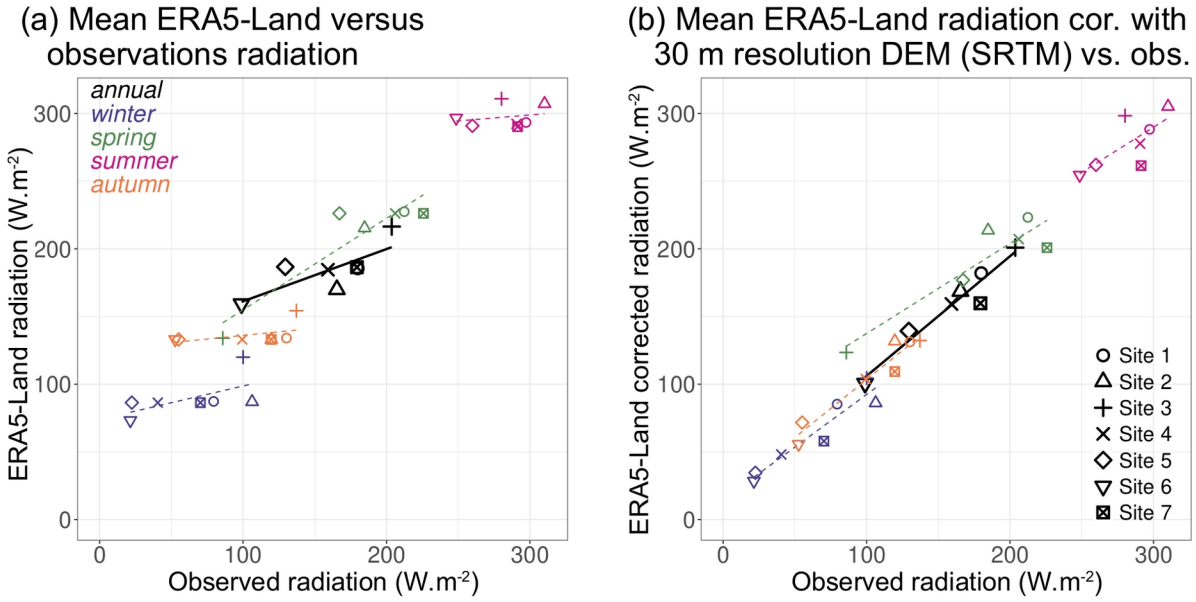

Figure 3: Comparison of the observed radiation with the ERA5-Land product (a) and with corrected radiation from ERA5-Land using 30 m resolution DEM (b). For each of the 7 points studied, the annual (in black) and seasonal (in colours) mean radiation ($W.m^{-2}$) are shown, as well as the linear regression line (equation, r^2 and RMSE, see table 2).

	ERA5-Land vs. observations			ERA5-Land corrected with 30 m resolution DEM vs. obs.		
	equation	r^2	RMSE	equation	r^2	RMSE
annual	y = 123+ 0.39 x	0.59	33.5	y = 18 + 0.89 x	0.93	8.6
winter	y = 74 + 0.25 x	0.37	37.7	y = 15 + 0.78 x	0.90	11.1
spring	y = 87 + 0.68 x	0.85	35.1	y = 71 + 0.67 x	0.85	22.7
summer	y = 272+ 0.09 x	0.05	24.6	y = 90 + 0.67 x	0.53	14.8
autumn	y = 125+ 0.11 x	0.21	45.3	y = 18 + 0.86 x	0.94	9.1

Table 2. Linear regression parameters and statistics (r^2 and RMSE, $W.m^{-2}$) for comparison of the observed radiation with the ERA5-Land product and with corrected radiation from ERA5-Land using 30 m DEM (see Fig. 3).

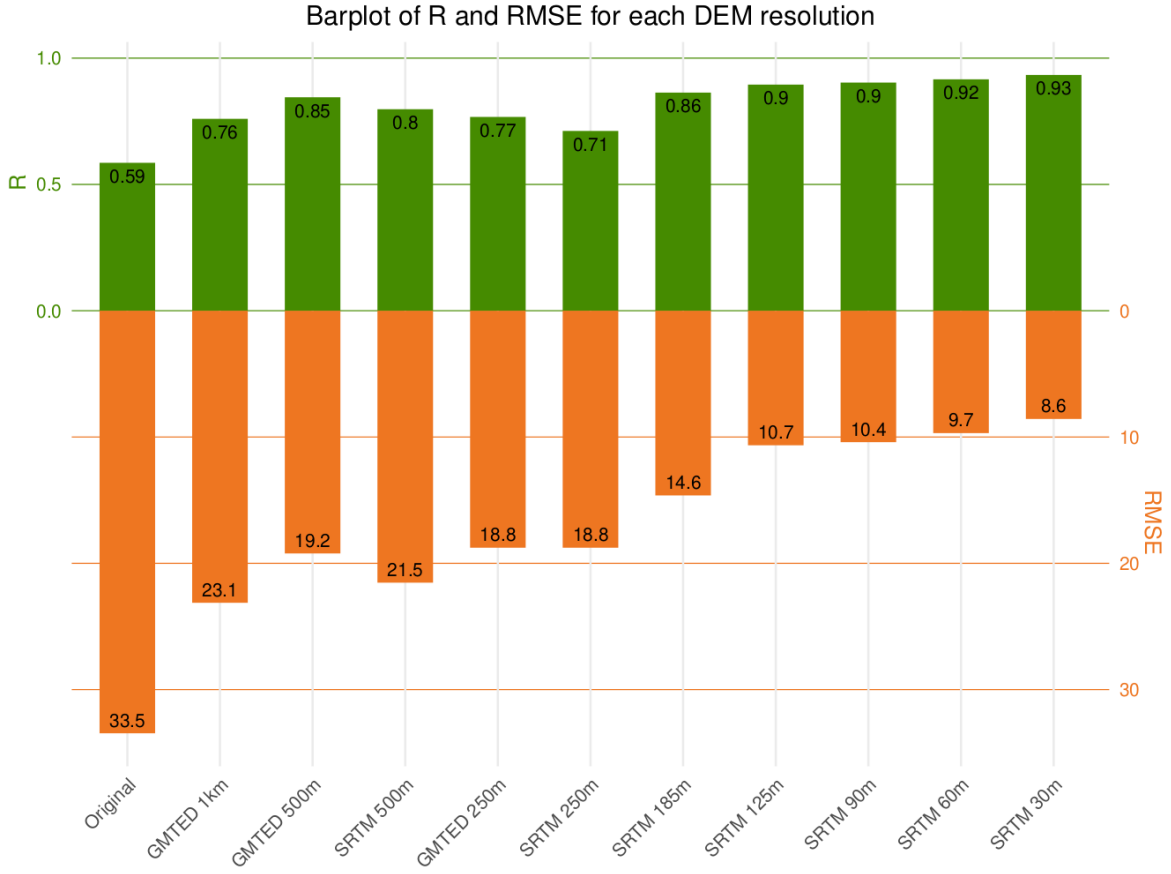

340 **Figure 4: Comparison of the performances of ERA5-Land product and corrected radiation from ERA5-Land using different DEMs with observed radiation. The annual correlation r^2 is represented in green and the RMSE ($W.m^{-2}$) in orange.**

Figure 5 depicts the global radiation values for two distinct sites during two different periods. Site 1 (refer to Table 1) represents a slightly south-facing location with little shade from topographical features, particularly evident in winter. Site 5, on the other hand, is situated on a north-facing slope (slightly west-facing) affecting sunlight exposure, especially during winter months. Two three-day periods were selected for analysis: one in summer (19-21 August 2016) to observe the impact during peak sun exposure (on the 21st), a cloudy day (the 20), and an intermediate day (the 19); and another in winter (12 to 14 January 2017, cloudless days) to assess the effect of the downscaling on low-inclination radiation in a mountainous region. Three types of radiation values are presented: observed values (Sect. 2.3), original ERA5-Land values (9 km resolution, tile indicated on Fig. 2), and values following the application of the radiation downscaling with the SRTM DEM (~30 m resolution) (as described in Sect. 2.1, but without "hillshading" function to be comparable with measurements which are made with sensors set horizontal). The presence of clouds was assessed with data combining high-resolution cloud information is directly inferred from satellite observations, such as the Copernicus Atmosphere Monitoring Service (CAMS) solar radiation time-series data (available on https://ads.atmosphere.copernicus.eu/stac-browser/collections/cams-solar-radiation-timeseries, last access the 22/10/2024), and are represented on Fig. S1. The difference between sky-view and all sky radiation indicates the presence of clouds.

At site 1 (Fig. 5.a-c), where surrounding topographical features have minimal impact on radiation, the values from ERA5-Land were close to the observations and there was no significant change after radiation downscaling. These trends held for both clear and cloudy days, and for both winter and summer periods. At site 5, disparities between original and corrected ERA5-Land values were more significant due to topographical influences than at site 1. In summer (Fig. 5.b), discrepancies existed between original and corrected ERA5-Land values. Corrected values accurately depict the evolution measured, especially the 21 August, and constantly more closely represented measured values, but still struggled to replicate sub-daily variations. Particularly, a dip in the curve around 10am appeared to be present on the 19, possibly indicating a shadow or the presence of localized clouds or fog, but not represented in the original and the corrected radiations. In winter (Fig. 5.d), downscaling markedly impacted radiation values, with corrected values nearly four times lower than ERA5-Land values at the northern site, closely aligning with observed values.

Note that if the effect of the slope and aspect on radiation intensity were activated in the script, the effect of the light intensity could increase in the corrected radiation on the south faces, mainly on clear days and in winter (e.g. +10 % for point 1). By contrast it could reduce the corrected radiation on cloud-free days (e.g. by a factor two for 21 August at point 5).

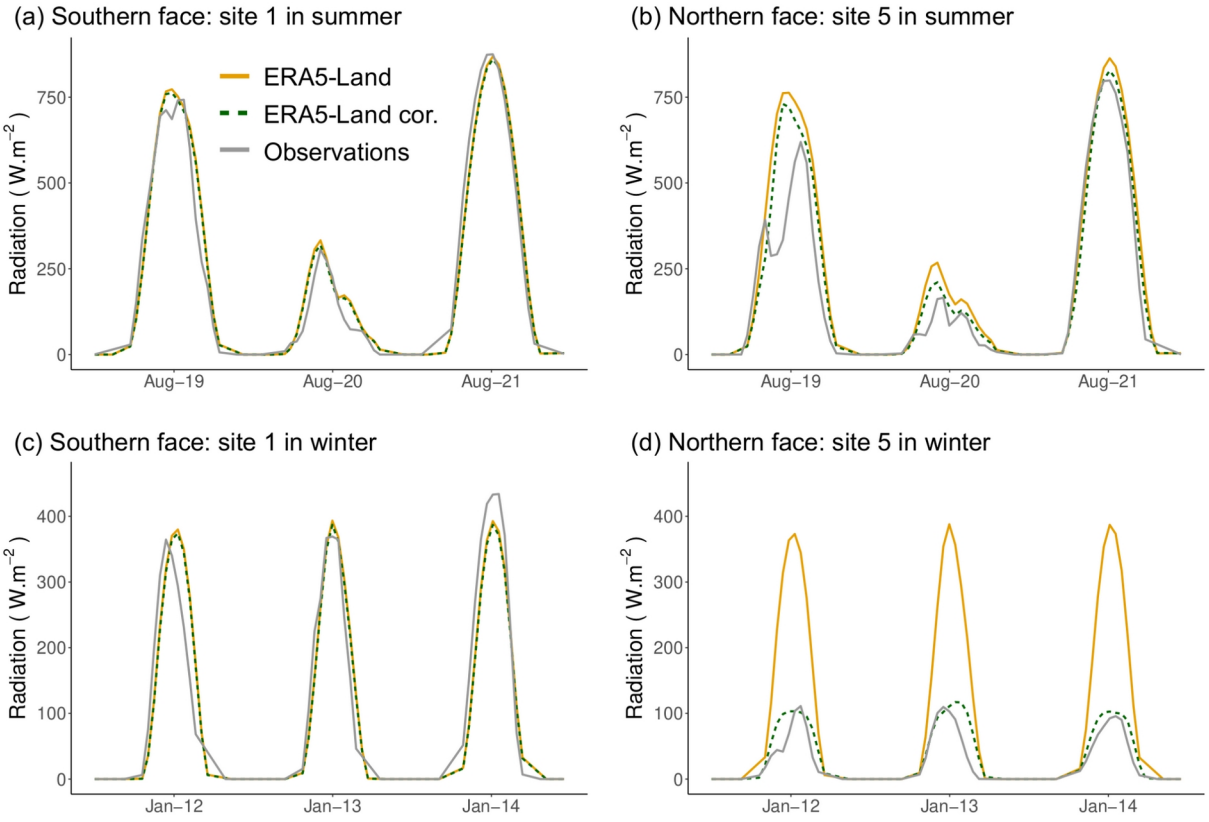

Figure 5: Radiation of original ERA5-Land data in orange, after downscaling with the SRTM DEM (30 m resolution) in dotted dark green and the observations in grey, for site 1 (a and b) and site 5 (c and d) and for two different dates: one in summer (19-21 August 2016 in a and c) and one in winter (12-14 January 2017 in b and d)

3.2 Application on Mont Ventoux massif

3.2.1 Heterogeneity of global radiation

Applying our approach across a heterogeneous geographical area illustrates the spatial and temporal variability in global radiation introduced by downscaling (Fig. 6).

Radiation downscaling exerted a clear impact in the mountainous region under study, halving original ERA5-Land global radiation. An evident differentiation emerged between south-facing slopes, which received more radiation, and north-facing slopes, which exhibited minimal radiation levels in winter (approaching zero). Mean radiation values decreased with increasing resolution of the three DEM used, indicating an average decrease of 10.7 % on 13 January 2017 and 5.9 % on 19 August 2016 when transitioning from the GMTED DEM at approximately 500 metres to the SRTM at approximately 30 metres resolution. Conversely, standard deviation increased with resolution, rising by 13.5 % and 30.0 %, respectively. During winter, the standard deviation was similar in magnitude of the mean due to low radiation values, whereas in summer, it accounted for 20 to 25 % of the mean.

These differences in standard deviation due to topography implied significant differences between the different DEMs, as well as with the original ERA5-Land values. For instance, the daily accumulation of radiation value recorded on January 13th was 7.3 MJ.m^{-2} in the reanalysis, whereas the maximum daily radiation reached 9.3 MJ.m^{-2} in the ERA5-Land tile with downscaling conducted using the 250 m DEM. Similarly, on January 13th (Fig. 6.b), the spatial pattern representing a denser "line" denoting stronger radiation values around 5.3° E and 44.19° N was relatively narrow with the 30 m DEM (approximately 200 meters wide), whereas it doubled in width with the 500 m DEM.

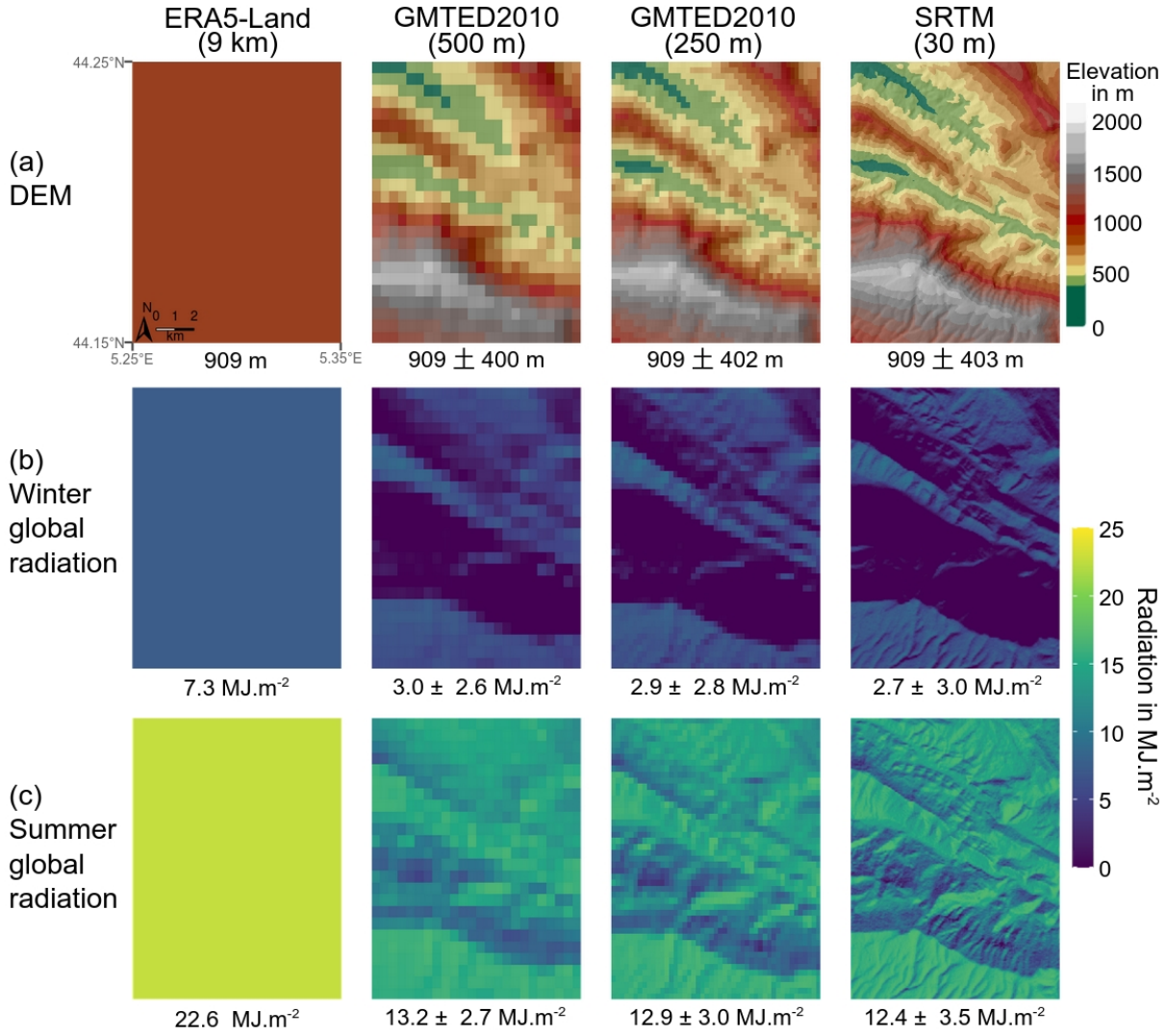

Figure 6: Global radiation from ERA5-Land and resulting from downscaling obtained from different resolution DEMs. (a) ERA5-Land tile (left) and DEM resolution (500, 250, and 30 metres, from left to right). Daily global radiation for two distinct dates, (b) in winter (13 January 2017) and (c) in summer (19 August 2016). Regional mean values and standard deviations are indicated on the bottom of each map.

3.2.2 Modelling the influence of radiation downscaling on vegetation function

Modifying radiation across the entire area according to each DEM had a tangible impact on the predictions of vegetation processes as presented on models output as shown in Fig. 7. In general, the simulations remained consistent across the studied area, despite potential variations introduced by the different topographies used during downscaling. With the three different downscaling (from 8 km to 500 m, 250 m and 30 m), there is a discernible reduction in Gross Primary Productivity (GPP) ranging between 5 % and 8 %, as well as in the risk of hydraulic failure, which decreases between 14 % and 23 %. Moreover, the standard deviation introduced between the values was quite significant, varying between 8 % and 13 % for the two outputs studied.

Upon comparing the patterns obtained with the corresponding DEMs, we observed that south-facing slopes tended to exhibit higher annual productivity (Fig. 7.b) but were susceptible to greater hydraulic stress (as indicated by darker colours in Fig. 7.c). Conversely, north-facing slopes generally manifested lower GPP as simulated by the CASTANEA model, yet exhibited a reduced risk of hydraulic failure.

To evaluate the potential impact of these discrepancies on drought-induced mortality, we computed the risk of hydraulic failure from the SurEau simulations. The relationship between mortality due to water stress and risk of hydraulic failure is often conceptualised as a threshold effect (Choat et al., 2018), although this notion is occasionally questioned (Hammond et al., 2021). Setting at 50% the risk of hydraulic failure threshold at which trees die, we obtained drought-induced mortality percentages in term of surface of 100 %, and 97 %, 98 % and 89 % for the original ERA5-Land tile, and the data downscaled to 500 m, 250 m and 30 m, respectively. Given that the total soil available water accessible for the trees used in this study came from a single value taken from the median over the area of the SoilGrids database (Poggio et al., 2021), and that this value is subject to uncertainty, these results must be compared relatively to each other.

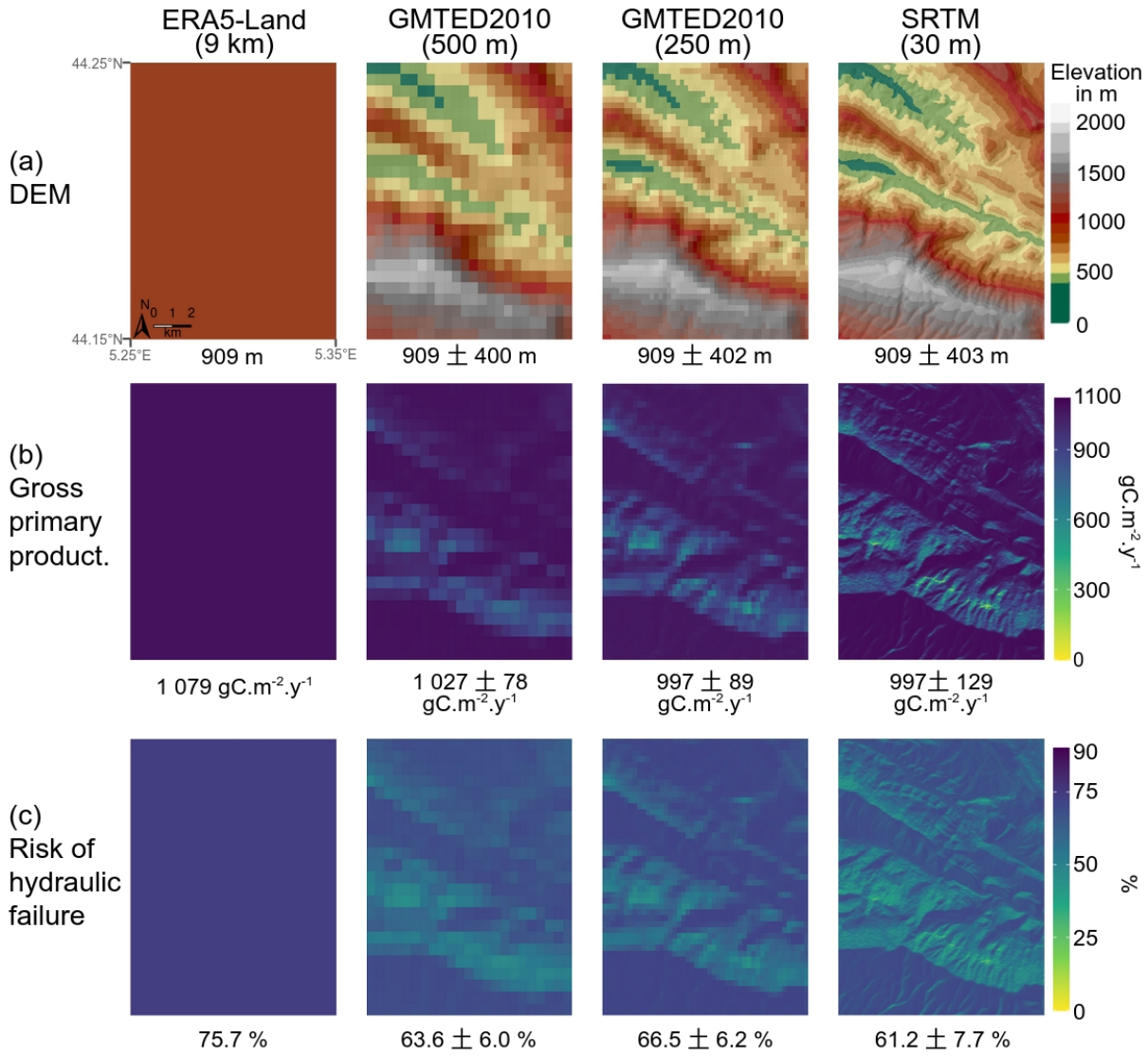

Figure 7: Gross primary productivity and risk of hydraulic failure simulated with, respectively, CASTANEA and SurEau, from ERA5-Land and resulting from global radiation downscaling obtained from different resolution DEMs. (a) ERA5-Land tile (left) and DEM resolution (500, 250, and 30 metres, from left to right). (b) Gross primary productivity simulated with CASTANEA. (c) Risk of hydraulic failure simulated with SurEau. Regional mean values and standard deviations are indicated on the bottom of each map.

4 Discussion

4.1 Performance of the downscaling method

The radiation downscaling method we present in this study significantly improved radiation predictions in mountainous regions compared to those provided by reanalysis products. More specifically, we demonstrated that accounting for the

impact of topography and distinguishing between direct and diffuse radiation allowed us to better capture seasonal radiation patterns. On the north-facing side of our study area, where global radiation is reduced due to the obstruction of direct sunlight by surrounding mountains, our downscaling method significantly lowered radiation levels, particularly during winter when the Sun is at its lowest position on the sky. Conversely, on the south-facing slopes, the steepness of the terrain and the more direct alignment with the sun resulted in increased radiation levels. This effect was also particularly pronounced in winter, when the Sun is lower in the sky but more favourably oriented towards these slopes. Consequently, our method represented the spatial heterogeneity of radiation that can be observed in complex terrain, significantly improving radiation estimations from larger scale renalysis products when a fine downscaling scale is chosen. This corroborates the results reported by other studies based on slope, aspect ratio and skyview, which indicate improved results after downscaling (Müller and Dieter, 2005; Senkova et al., 2007; Buzzi, 2008). Nevertheless, none of these studies combines both high spatial (here ~30 m) and temporal resolution (hourly). Furthermore, by comparing precisely resolved data combining high-resolution cloud information is directly inferred from satellite observations (Fig. S1), the quality of our results is confirmed. While in summer, the CAMS data are consistent with both our results and the observations, in winter the results presented in Fig. 5 are much closer to the observations at the south-facing site, while at the north-facing site the topographical correction allows us to be very close to the observations, whereas the CAMS data are very far from them.

Our analysis showed a clear but non-uniform improvement in radiation estimates as the resolution of our downscaling method increased. While no continuous improvement was observed at resolutions coarser than 250 m, a gradual improvement emerged for finer resolutions, down to 30 m. This suggests that topoclimatic processes, such as the effects of topography on local radiation patterns, operate at these finer spatial scales, highlighting the importance of high-resolution estimations for accurately representing the influence of terrain on local climate. On the other hand, our results for resolutions coarser than 250 m, suggest that insufficient improvement in resolution during the downscaling introduces some variance (due to the inherent uncertainty of the method and additional processing of the variable) which can mitigate improvements in radiation representation at the site level.

As we clearly observed in our study area, the impact of radiation downscaling was primarily observed in regions with significant shadow casting, whose effect becomes more pronounced as the Sun's zenithal angle decreases. Due to energy equilibrium and conservation at large scale, this implies that an increase in radiation was observed on south-facing slopes or on mountaintops. This effect was particularly pronounced when the angle between the incoming direct radiation and the aspect of the relief (slope and azimuth) approaches perpendicularity relative to a flat surface. However, it's worth noting that our study area is not characterised by extremely steep mountains, so these effects are primarily observed on moderate slopes. In regions with much steeper terrain, we would expect the impact of topography on radiation to be even more pronounced, especially in valley bottoms, where shading effects could remain significant even on south-facing slopes.

An important source of uncertainty in our radiation downscaling method likely stems from the way global radiation is split into direct and diffuse components using the ratio of R_g to R_0 as a proxy for cloud cover. This approach cannot capture the spatial and temporal heterogeneity of cloud cover, which can be especially significant in mountainous regions (Buzzi, 2008). This explains why, while daily patterns were effectively estimated, sub-daily variations were more difficult to capture. For instance, in Figure 5.b, the dip around 10 a.m. the 19 August may suggest the presence of microclimatic conditions, such as clouds or fog, an effect not considered in our downscaling method. Actually, the original ERA5-Land data cannot depicts the presence of isolated clouds as it happens on the day presented for summer in Figure 5 as they provide averaged values of incoming radiation over the whole mesh area. Such occurrences could be tracked by using higher resolution solar radiation products such as those obtained from satellite imagery and in particular geostationary satellites with a spatial resolution in the order of 2 to 3 km and a time resolution between 5 and 15 minutes (ex. Roerink et al. 2012, Bojanowski et al. 2014).Indeed, this dip may be associated with the presence of small clouds or fog capping Mont Ventoux during morning, signalled by the drop-out between the CAMS clear-sky and all sky (Fig. S1). Similarly, the small dip observed shortly after in Figure 5.a is actually related to the presence of small clouds of fog capping Mont Ventoux during morning, moving from one site to another. Further analyses with such data could help quantify the extent to which this effect contributes to overall uncertainty of our methodology.

4.2 Implications of radiation downscaling for modelling studies and perspectives of improvements

Using downscaled radiation estimations as input in two process-based forest models provides an overview of the impact that radiation downscaling can have on different forest processes, namely Gross Primary Production (GPP) or drought-induced mortality. Overall, our results revealed that the effects of topography on local radiation patterns can have important implications on these key forest processes. For instance, when considering processes that are based on thresholds, such as the drought-induced mortality associated with risk of hydraulic failure, the mortality rate was reduced from 100 % to 89 %. As could be deduced from the results on radiation alone, the impact of downscaling on GPP and drought-induced mortality was most pronounced in areas with significant topographic features, such as north-facing slopes due to shading or south-facing slopes due to increased radiation levels.

While the effect of topography on forest ecological processes is often assessed through its impact on temperature or precipitation patterns (Randin et al., 2009), these results suggest that spatial heterogeneity of radiation, through its interaction with topography, seems also crucial for accurately assessing ecological responses and potential threshold effects in complex terrain. Future studies could benefit from integrating our radiation downscaling method to improve predictions of forest functioning at a very local scale.

However, these findings should be interpreted with caution as, in our study, only solar radiation was downscaled, leading to potential decoupling with the other forcing variables (temperature, humidity, precipitation and wind). Downscaling methods

exist for these variables, for example the use of simple adiabatic gradient for temperature, or kriging methods or high resolution radar data for rainfall (Liston and Elder 2006, Davy & Kusch, 2021) or dynamic models (Maraun et al., 2010), but they are not consistent with the one proposed here. We therefore need to check the consistency of each of the downscaling methods, or evaluate if it is possible to integrate this method or its outputs to downscale other variables with other methods. Indeed, it is important to start from physically-consistent data: in this case ERA5-Land, but which can be adapted, as the method can be adapted to any global (or direct and indirect) radiation input. Finally, the method developed here is only applicable to shortwave radiation, which is the only radiation currently required by the models used. Nevertheless, the principle of the method presented here could be used as a starting point for downscaling longwave radiation. Following the principle presented in Senkova et al (2007), the method used for diffuse radiation (based on the skyview) could be partially applicable to longwave radiation. If it is considered as isotropic, incoming atmospheric radiation could be downscaled directly on the basis of the methodology used to downscale diffuse incoming solar radiation. However, it would be necessary to account for the radiation emitted by land surfaces in view as emitted radiation from the surface is usually significantly higher than atmospheric radiation (this would be particularly true for cloudless skies). This would require the knowledge of the surface temperatures of the surrounding areas, but it is also important to recall that the net longwave radiation has a significantly lower impact than the net shortwave radiation on the surface energy balance (ex. Mira et al. 2016).

5 Conclusion

In this study, we developed a process-based method to downscale global radiation data made on flat surfaces, such as coarse spatial resolution global reanalysis data. The method builds upon existing research and goes further than traditional process-based radiation downscaling methods, by accounting for the shadowing effect on direct radiation and for the skyview factor on diffuse radiation (Piedallu & Gégout, 2008). The recent ERA5-Land hourly data available at 9 km resolution was used to compare on Mont Ventoux the impact of radiation downscaling computed from different digital elevation models.

The radiation downscaling method effectively captured the overall trend of radiation distribution across mountainous regions. Agreement with observations was improved for downscaled radiation compared to original ERA5-Land data, especially during winter months, due to the higher zenithal angle. This improvement was particularly significant and increased gradually after a certain spatial resolution (~ 150 m). The implications of downscaling for modelling studies was further investigated using two different process-based models representing gross primary productivity and risk of hydraulic failure. The impact of downscaling on those variables was most pronounced in areas with significant topographic features, such as mountainous regions or canyons. Assessing the spatial heterogeneity of radiation, through its interaction with topography, is crucial for accurately addressing ecological responses and potential threshold effects in complex terrain.

The method can be applied at any resolution, depending on the choice of the DEM. Moreover, it can be applied to any type of radiation data, making it applicable to any region in the world and to historical periods as well as future projections. Finally, the method could involve other types of climatic data from the same input dataset, such as temperature or precipitation, thereby ensuring physical consistency between the variables. In the future such methods could be included in more generic climate downscaling tools (e.g. Meteoland, De Cáceres et al., 2018) to facilitate the application of process based models at fine resolution.

Code availability

The scripts corresponding to the method developed in this article is available on GitLab at https://forgemia.inra.fr/urfm/modeldata_toolkit with the prefix "RadDownscaling" (commit 8c4509c3; tag Biogeosciences_Druel&al2024).

The SurEau model code presented in section 2.4 and whose results are presented in section 3.2 is available on GitLab at https://forgemia.inra.fr/urfm/sureau (commit ca19abfb), while the CASTANEA version is available on the capsis platform (https://capsis.cirad.fr/, lasted access the 12/06/2024) and can be downloaded from the "download" menu.

Data availability

Data from Mont Ventoux (2016-2017) at the seven sites are provided by URFM-INRAE Avignon. The full dataset and site information can be accessed from https://doi.org/10.57745/B22AUG.

DEM data are freely accessible and can be downloaded from https://earthexplorer.usgs.gov/ (last accessed 12/06/2024): the Global Multi-resolution Terrain Elevation Data 2010 (GMTED2010) (https://doi.org/10.5066/F7J38R2N) and the Shuttle Radar Topography Mission (SRTM) 1 Arc-Second Global (https://doi.org/10.5066/F7PR7TFT).

Climate ERA5-Land data (https://doi.org/10.24381/cds.e2161bac), including global radiation, are provided by Copernicus and can be directly downloaded from https://cds.climate.copernicus.eu/cdsapp#!/dataset/reanalysis-era5-land?tab=form (last accessed 12/06/2024).

Author contribution

Druel, A., Ruffault, J., Davi, H. and Martin-StPaul, N.K. designed the research and performed the research. Druel, A. developed the scripts and the figures. Marloie, O. and Martin-StPaul, N.K. collected the data on Mont Ventoux. Druel, A., Ruffault, J., Davi, H., De Cáceres, M., Mouillot, F., François, C. and Martin-StPaul, N.K. interpreted the results. Druel, A. led the writing of the manuscript with inputs from Ruffault, J., Chanzy, A., Marloie, O., De Cáceres, M., Mouillot, F.,

François, C., Soudani, K., and Martin-StPaul, N.K. Finally, Druel, A., Ruffault, J., Olioso, A., and Martin-StPaul, N.K., were particularly involved in the review.

Competing interests

The authors declare that they have no conflict of interest.

Acknowledgements

This project received funding from the European Union's Horizon 2020 research and innovation program under Grant Agreement No. 862221 (FORGENIUS). The authors would also like to thank William Brunetto (URFM, INRAE, Avignon, France) for his help with data acquisition on Mont Ventoux and Deborah Verfaillie for her help with proofreading.

References

Austin, M.P., Nicholls, A.O. and Margules, C.R.: Measurement of the realised qualitative niche: Environmental niches of five Eucalyptus species. *Ecological Monographs*, 60(2): 161-177, https://doi.org/10.2307/1943043, 1990.

Bailey, M. D., Nychka, D., Sengupta, M., Habte, A., Xie, Y., and Bandyopadhyay, S.: Regridding uncertainty for statistical downscaling of solar radiation. *Adv. Stat. Clim. Meteorol. Oceanogr.*, 9, 103–120, https://doi.org/10.5194/ascmo-9-103-2023, 2023.

Bedia, J., Herrera, S. and Gutiérrez, J.M.: Dangers of Using Global Bioclimatic Datasets for Ecological Niche Modeling. Limitations for Future Climate Projections. *Global and Planetary Chang*e, 107, 1-12, http://dx.doi.org/10.1016/j.gloplacha.2013.04.005, 2013.

Bird, R. E., and Hulstrom, R. L.: A simplified clear sky model for direct and diffuse insolation on horizontal surfaces. *Solar Energy Research Institute*, TR-642-761, 1981.

Bojanowski, J.S., Vrieling, A., and Skidmore, A.K.: A comparison of data sources for creating a long-term time series of daily gridded solar radiation for Europe. *Sol. Energy*, 99, 152–171, http://dx.doi.org/10.1016/j.solener.2013.11.007, 2014.

Bramer, I., Anderson, B.J., Bennie, J., Bladon, A.J., De Frenne, P., Hemming, D., Hill, R.A., Kearney, M.R., Körner, C.,Korstjens, A.H., Lenoir, J., Maclean, I.M.D., Marsh, C.D., Morecroft, M.D., Ohlemüller, R., Slater, H.D., Suggitt, A.J., Zellweger, F. and Gillingham, P.K.: Advances in monitoring and modelling climate at ecologically relevant scales. *Advances in Ecological Research*, 58, 101–161.https://doi.org/10.1016/bs.aecr.2017.12.005, 2018.

Brun, P., Zimmermann, N. E., Hari, C., Pellissier, L. and Karger, D. N.: CHELSA-BIOCLIM+ A novel set of global climate-related predictors at kilometre-resolution. *EnviDat.*, https://www.doi.org/10.16904/envidat.332, 2022.

Buzzi, M.: (2008). Challenges in operational numerical weather prediction at high resolution in complex terrain. ETH Zürich, PhD thesis, Veröffentlichung MeteoSchweiz Nr. 80, ISSN: 1422-1381, https://doi.org/10.3929/ethz-a-005698833, 2008.

Cailleret, M. and Davi, H.: Effects of climate on diameter growth of co-occurring *Fagus sylvatica* and *Abies alba* along an altitudinal gradient. *Trees*, 25:265–276. https://doi.org/10.1007/s00468-010-0503-0, 2011.

Cailleret M., Nourtier M., Amm A., Durand-Gillmann M. and Davi H.: Drought-induced decline and mortality of silver fir differ among three sites in Southern France. *Annals of Forest Science*, 71, 643–657, 2013.

Carroll, C., Zielinski, W.J. and Noss, R.F.: Using presence-absence data to build and test spatial habitat models for the Fisher in the Klamath region, U.S.A. *Conservation Biology*, 13(6): 1344-1359, https://doi.org/10.1046/j.1523-1739.1999.98364.x, 1999.

Clark, D.B., Palmer, M.W. and Clark, D.A.: Edaphic factors and the landscape-scale distributions of tropical rain forest trees. *Ecology*, 80(8): 2662-2675, https://doi.org/10.1890/0012-9658(1999)080[2662:EFATLS]2.0.CO;2, 1999.

Choat, B., Brodribb, T. J., Brodersen, C. R., Duursma, R. A., López, R. and Medlyn, B. E.: Triggers of tree mortality under drought. *Nature*, 558(7711), 531–539. https://doi.org/10.1038/s41586-018-0240-x, 2018.

Churkina, G., and Running, S. W.: Contrasting Climatic Controls on the Estimated Productivity of Global Terrestrial Biomes. *Ecosystems*, 1(2), 206–215. https://doi.org/10.1007/s100219900016, 1998.

Cochard, H., Pimont, F., Ruffault, J. & Martin-StPaul, N.: SurEau: a mechanistic model of plant water relations under extreme drought. *Ann. For. Sci.*, 78, https://doi.org/10.1007/s13595-021-01067-y, 2021.

Coddington, O., Lean, J. L., Pilewskie, P., Snow, M. and Lindholm, D.: A Solar Irradiance Climate Data Record. *Bull. Amer. Meteor. Soc.*, 97, 1265–1282, https://doi.org/10.1175/BAMS-D-14-00265.1, 2016.

Danielson, J.J., and Gesch, D.B.: Global multi-resolution terrain elevation data 2010 (GMTED2010): U.S. Geological Survey Open-File Report 2011–1073, 26 p., https://doi.org/10.5066/F7J38R2N (Downloaded on https://earthexplorer.usgs.gov/ the 15-10-2021), 2011.

Davi, H., Dufrêne, E., Granier, A., Le Dantec, V., Barbaroux, C., François, C. and Bréda, N.: Modelling carbon and water cycles in a beech forest: Part II.: Validation of the main processes from organ to stand scale. *Ecological Modelling*, 185, 387–405. doi:10.1016/j.ecolmodel.2005.01.003, 2005.

Davi, H., Dufrêne, E., Francois, C., Le Maire, G., Loustau, D., Bosc, A., Rambal, S., Granier A. and Moors E.: Sensitivity of water and carbon fluxes to climate changes from 1960 to 2100 in European forest ecosystems. *Agric. For. Meteorol.*, 141, 35–56, https://doi.org/10.1016/j.agrformet.2006.09.003, 2006.

Davi, H. and Cailleret, M.: Assessing drought-driven mortality trees with physiological process-based models. *Agricultural and Forest Meteorology*, 232, 279–290, https://doi.org/10.1016/j.agrformet.2016.08.019, 2017.

Davy, R. and Kusch, E.: Reconciling high resolution climate datasets using KrigR. *Environ. Res. Lett.*, 16, 124040, https://doi.org/10.1088/1748-9326/ac39bf, 2021.

De Cáceres, M., Martínez-Vilalta, J., Coll, L., Llorens, P., Casals, P., Poyatos, R., Pausas, J.G. and Brotons, L.: Coupling a water balance model with forest inventory data to predict drought stress: the role of forest structural changes vs. climate changes. *Agricultural and Forest Meteorology*, 213: 77-90, https://doi.org/10.1016/j.agrformet.2015.06.012, 2015.

De Cáceres, M., Martin-StPaul, N., Turco, M., Cabon, A. and Granda, V.: Estimating daily meteorological data and downscaling climate models over landscapes. *Environmental Modelling and Software*, 108: 186-196, doi:10.1016/j.envsoft.2018.08.003, 2018.

De Cáceres M, Molowny-Horas R, Cabon A, Martínez-Vilalta J, Mencuccini M, García-Valdés, R., Nadal-Sala, D., Sabaté, S., Martin-StPaul, N., Morin, X., D'Adamo, F., Batllori, E. and Améztegui, A.: MEDFATE 2.9.3: A trait-enabled model to simulate Mediterranean forest function and dynamics at regional scales. *Geoscientific Model Development*, 16, 3165–3201, https://doi.org/10.5194/gmd-16-3165-2023, 2023.

De Jong, J.B.R.M.: Een karakterisering van de zonnestraling (A characterization of solar radiation) in Nederland. Doctoral report, Eindhoven University of Technology, Netherlands, 97 + 67 pp., 1980.

Delpierre, N., Soudani, K., Franc¸ois, C., Le Maire, G., Bernhofer, C., Kutsch, W., Misson, L., Rambal, S., Vesala, T., and Dufrêne, E.: Quantifying the influence of climate and biological drivers on the interannual variability of carbon exchanges in European forests through process-based modelling. *Agric. For. Meteorol.*, 154–155, 99–112, https://doi.org/10.1016/j.agrformet.2011.10.010, 2012.

Dirnbock, T., Dullinger, S., Gottfried, M., Ginzler, C. and Grabherr, G.: Mapping alpine vegetation based on image analysis, topographic variables and Canonical Correspondance Analysis. *Applied Vegetation Science*, 6: 85-96, https://doi.org/10.1111/j.1654-109X.2003.tb00567.x, 2003.

Dubayah, R. and Loechel, S.: Modeling topographic solar radiation using GOES data. J. *Appl. Meteor.*, 36, 141–154, https://doi.org/10.1175/1520-0450(1997)036<0141:MTSRUG>2.0.CO;2, 1997.

Dufrêne, E., Davi, H., François, C., Maire, G. l., Dantec, V. L., and Granier, A.: Modelling carbon and water cycles in a beech forest: Part I: Model description and uncertainty analysis on modelled NEE. *Ecol. Model.*, 185, 407–436, https://doi.org/10.1016/j.ecolmodel.2005.01.004, 2005.

Fealy, R. and Sweeney, J.: Statistical downscaling of temperature, radiation and potential evapotranspiration to produce a multiple GCM ensemble mean for a selection of sites in Ireland. *Irish Geography*, 41:1, 1-27, DOI: https://doi.org/10.1080/00750770801909235, 2008.

Fisher, J. B., Whittaker, R. J., and Malhi, Y.: ET come home: Potential evapotranspiration in geographical ecology: ET come home. *Global Ecology and Biogeography*, 20(1), 1–18. https://doi.org/10.1111/j.1466-8238.2010.00578.x, 2011.

Franklin, J.: Predicting the distribution of shrub species in southern California from climate and terrain-derived variables. *Journal of Vegetation Science*, 9(5): 733-748, https://doi.org/10.2307/3237291, 1998.

Corripio, J.G.: insol: Solar Radiation. R package version 1.2.2, https://www.meteoexploration.com/R/insol/ (last access 27/05/2024), 2020.

Granier, A., Breda, N., Biron, P. and Villette, S.: A lumped water balance model to evaluate duration and intensity of drought constraints in forest stands. *Ecol. Model.*, 116:269–283, https://doi.org/10.1016/S0304-3800(98)00205-1, 1999.

Granier, A., Reichstein, M., Bréda, N., Janssens, I. A., Falge, E., Ciais, P., Grünwald, T., Aubinet, M., Berbigier, P., Bernhofer, C., Buchmann, N., Facini, O., Grassi, G., Heinesch, B., Ilvesniemi, H., Keronen, P., Knohl, A., Köstner, B., Lagergren, F., Lindroth, A., Longdoz, B., Loustau, D., Mateus, J., Montagnani, L., Nys, C., Moors, E.J., Papale, D., Peiffer, M., Pilegaard, K., Pita, G., Pumpanen, J., Rambal, S., Rebmann, C., Rodrigues, A., Seufert, G., Tenhunen, J., Vesala, T. and Wang, Q.: Evidence for soil water control on carbon and water dynamics in European forests during the extremely dry year: 2003. *Agricultural and Forest Meteorology*, 143(1-2), 123-145. https://doi.org/10.1016/j.agrformet.2006.12.004, 2007.

Hammond, W. M., Yu, K., Wilson, L. A., Will, R. E., Anderegg, W. R. L. and Adams, H. D.: Dead or dying? Quantifying the point of no return from hydraulic failure in drought-induced tree mortality. *New Phytologist*, 223(4), 1834–1843, https://doi.org/10.1111/nph.15922, 2019.

Hernanz, A., Correa, C., Domínguez, M., Rodríguez-Guisado, E. and Rodríguez-Camino, E.: Comparison of machine learning statistical downscaling and regional climate models for temperature, precipitation, wind speed, humidity and radiation over Europe under present conditions. *International Journal of Climatology*, 43, 13, 6065-6082, https://doi.org/10.1002/joc.8190, 2023.

Hijmans, R.J., Cameron, S.E., Parra, J.L., Jones, P.G. and Jarvis, A.: Very high-resolution interpolated climate surfaces for global land areas. *International Journal of Climatology*, 25(15):1965-1978, https://doi.org/10.1002/joc.1276, 2005.

Jean, F., Davi, H., Oddou-Muratorio, S., Fady, B., Scotti, I., Scotti-Saintagne, C., Ruffault, J., Journe, V., Clastre, P., Marloie, O., Brunetto, W., Correard, M., Gilg, O., Pringarve, M., Rei, F., Thevenet, J., Turion, N. and Pichot, C.: A 14-year series of leaf phenological data collected for European beech (*Fagus sylvatica L.*) and silver fir (*Abies alba Mill.*) from their geographic range margins in south-eastern France. *Annals of Forest Science*, (2023)80:35, https://doi.org/10.1186/s13595-023-01193-9, 2023.

Klein, T.: The variability of stomatal sensitivity to leaf water potential across tree species indicates a continuum between isohydric and anisohydric behaviours. *Funct. Ecol.*, 28, 1313–1320, https://doi.org/10.1111/1365-2435.12289, 2014.

Klucher, T.M.: Evaluation of models to predict insolation on tilted surfaces. Division of *solar energy,* N.A.S.A. TM-78842, https://doi.org/10.1016/0038-092X(79)90110-5, 1978.

Lander, T.A., Klein, E.K., Roig, A. and Oddou-Muratorio, S.: Weak founder effects but significant spatial genetic imprint of recent contraction and expansion of European beech populations. *Heredity (Edinb)*, 126(3):491-504, doi: 10.1038/s41437-020-00387-5, 2021.

Liston, G.E. and Elder, K.: A Meteorological Distribution System for High-Resolution Terrestrial Modeling (MicroMet). *Journal of Hydrometeorology*, 7-2, 217-234, https://doi.org/10.1175/JHM486.1, 2006.

Maraun, D., Wetterhall, F., Ireson, A., Chandler, R., Kendon, E. et al.: Precipitation downscaling under climate change: Recent developments to bridge the gap between dynamical models and the end user. *Reviews of Geophysics*, American Geophysical Union, 48 (3), https://doi.org/10.1029/2009RG000314, 2010.

Martin-StPaul, N., Delzon, S. and Cochard, H.: Plant resistance to drought depends on timely stomatal closure. *Ecology Letters*, 20(11), 1437–1447. https://doi.org/10.1111/ele.1285, 2017.

Martin-StPaul, N., Ruffault, J., Guillemot, J., Barbero, R., Cochard, H., Cailleret, M., Cáceres, M. D., Dupuy, J.-L., Pimont, F., Torres-Ruiz, J. M., and Limousin, J.-M.: How much does VPD drive tree water stress and forest disturbances? *Authorea,* Preprints. https://doi.org/10.22541/au.168147010.01270793/v1, 2023.

Meentemeyer, R.K., Moody, A. and Franklin, J.: Landscape-scale patterns of shrub-species abundance in California chaparral: The role of topographically mediated resource gradients. *Plant Ecology*, 156: 19-41, https://doi.org/10.1023/A:1011944805738, 2001.

Mira, M., Olioso, A., Gallego-Elvira, B., Courault, D., Garrigues, S., Marloie, O., Hagolle, O., Guillevic, P., and Boulet, G.: Uncertainty assessment of surface net radiation derived from Landsat images. *Remote sensing of Environment*, 175, 251–270. http://dx.doi.org/10.1016/j.rse.2015.12.054, 2016.

Monteith, J. L.: Evaporation and surface temperature. *Quarterly Journal of the Royal Meteorological Society*, 107(451), 1–27. https://doi.org/10.1002/qj.49710745102, 1981.

Moreno, M., Simioni, G., Cailleret, M., Ruffault, J., Badel, E., Carrière, S., Davi, H., Gavinet, J., Huc, R., Limousin, J.-M., Marloie, O., Martin, L., Rodríguez-Calcerrada, J., Vennetier, M. and Martin-StPaul, N.: Consistently lower sap velocity and growth over nine years of rainfall exclusion in a Mediterranean mixed pine-oak forest. *Agricultural and Forest Meteorology*, 308–309, 108472. https://doi.org/10.1016/j.agrformet.2021.108472, 2021.

Müller, M. D. and Scherer, D.: A grid- and subgrid-scale radiation parametrization of topographic effects for mesoscale weather forecast models. *Monthly Weather Review*, 133, 1431–1442, https://doi.org/10.1175/MWR2927.1, 2005.

Muñoz-Sabater, J., Dutra, E., Agustí-Panareda, A., Albergel, C., Arduini, G., Balsamo, G., Boussetta, S., Choulga, M., Harrigan, S., Hersbach, H., Martens, B., Miralles, D. G., Piles, M., Rodríguez-Fernández, N. J., Zsoter, E., Buontempo, C., and Thépaut, J.-N.: ERA5-Land: a state-of-the-art global reanalysis dataset for land applications. *Earth Syst. Sci. Data*, 13, 4349–4383, https://doi.org/10.5194/essd-13-4349-2021, 2021.

Oliphant, A. J., & Stoy, P. C.: An evaluation of semiempirical models for partitioning photosynthetically active radiation into diffuse and direct beam components. Journal of GeophysicalResearch: *Biogeosciences*, 123, 889–901, https://doi.org/10.1002/2017JG004370, 2018.

Patsiou, T.S., Conti, E., Zimmermann, N.E., Theodoridis, S. and Randin, C.F.: Topo-climatic microrefugia explain the persistence of a rare endemic plant in the Alps during the last 21 millennia. *Global Change Biology*, 20(7):2286–2300, https://doi.org/10.1111/gcb.12515, 2014.

Piedallu, C. and Gégout, J.-C.: Multiscale computation of solar radiation for predictive vegetation modelling. *Ann. For. Sci.*, 64, 899-909, DOI: 10.1051/forest:2007072, 2007.

Piedallu, C. and Gégout, J-C.: Efficient assessment of topographic solar radiation to improve plant distribution models. *Agricultural and Forest Meteorology*, 148 (11), pp.1696-1706., https://doi.org/10.1016/j.agrformet.2008.06.001, 2008.

Pierce, K.B., Lookingbill, T. and Urban, D.: A simple method for estimating potential relative radiation (PRR) for landscape-scale vegetation analysis. *Landscape Ecology*, 20(2): 137-147, https://doi.org/10.1007/s10980-004-1296-6, 2005.

Poggio, L., De Sousa, L. M., Batjes, N. H., Heuvelink, G. B. M., Kempen, B., Ribeiro, E., and Rossiter, D.: SoilGrids 2.0: Producing soil information for the globe with quantified spatial uncertainty. *Soil*, 7(1), 217–240. doi: 10.5194/soil-7-217-2021, 2021.

Randin, C. F., Engler, R., Normand, S., Zappa, M., Zimmermann, N. E., Pearman, P. B., Vittoz, P., Thuiller, W. and Guisan, A.: Climate change and plant distribution: local models predict high-elevation persistence. *Global Change Biology*, 15(6), 1557-1569. https://doi.org/10.1111/j.1365-2486.2008.01766.x, 2009.

Roderick, M. L.: Estimating the diffuse component from daily and monthly measurements of global radiation. *Agricultural and Forest Meteorology*, 95, 169-185, https://doi.org/10.1016/S0168-1923(99)00028-3, 1999.

Roerink, G.J., Bojanowski, J.S., de Wit, A.J.W., Eerens, H., Supit, I., Leo, O. and Boogaard, H.L.: Evaluation of MSG-derived global radiation estimates for application in a regional crop model. *Agric. For. Meteorol.*, 160, 36-47, https://doi.org/10.1016/j.agrformet.2012.02.006, 2012.

Ruffault, J., Martin-StPaul, N.K., Rambal, S. et Mouillot, F.: Differential regional responses in drought length, intensity and timing to recent climate changes in a Mediterranean forested ecosystem. *Climatic Change*, 117, 103–117, https://doi.org/10.1007/s10584-012-0559-5, 2013.

Ruffault, J., Pimont, F., Cochard, H., Dupuy, J.-L., and Martin-StPaul, N.: SurEau-Ecos v2.0: a trait-based plant hydraulics model for simulations of plant water status and drought-induced mortality at the ecosystem level, *Geosci. Model Dev.*, 15, 5593–5626, https://doi.org/10.5194/gmd-15-5593-2022, 2022.

Ruffault, J., Limousin, J-.M., Pimont, F., Dupuy, J-.L., De Cáceres, M., Cochard, H., Mouillot, F., Blackman, C.J., Torres-Ruiz, J.M., Parsons, R.A., Moreno, M., Delzon, S., Jansen, S., Olioso, A., Choat, B. and Martin-StPaul, N.: Plant hydraulic modelling of leaf and canopy fuel moisture content reveals increasing vulnerability of a Mediterranean forest to wildfires under extreme drought. *New Phytologist*, 237, 4, 1256-1269, https://doi.org/10.1111/nph.18614, 2023.

Senkova, A. V., Rontu, L., and Savijärvi, H.: Parametrization of orographic effects on surface radiation in HIRLAM. *Tellus A: Dynamic Meteorology and Oceanography*, 59:3, 279-291, https://doi.org/10.1111/j.1600-0870.2007.00235.x, 2007

Spitters, C.J.T., Toussaint, H.A.J.M., and Goudriaan, J.: Separating the diffuse and direct component of global radiation and its implications for modeling canopy photosynthesis Part I. Components of incoming radiation. *Agr. and Forest Met.*, 38(1-3), 217-229, https://doi.org/10.1016/0168-1923(86)90060-2, 1986.

Shuttle Radar Topography Mission (SRTM): 1 Arc-Second Global (2013). https://doi.org/10.5066/F7PR7TFT (Downloaded on https://earthexplorer.usgs.gov/ the 15-10-2021), 2013.

Stéfanon, M., Martin-StPaul, N. K., Leadley, P., Bastin, S., Dell'Aquila, A., Drobinski, P., and Gallardo, C.: Testing climate models using an impact model: What are the advantages? *Climatic Change*, 131(4), 649–661, https://doi.org/10.1007/s10584-015-1412-4, 2015.

Tappeiner, U., Tasser, E. and Tappeiner, G.: Modelling vegetation patterns using natural and anthropogenic influence factors: preliminary experience with a GIS based model applied to an Alpine area. *Ecological Modelling*, 113(1-3): 225-237, https://doi.org/10.1016/S0304-3800(98)00145-8, 1998.

Widén, J. and Munkhammar, J.: Solar Radiation Theory. *Uppsala University, Department of Engineering Sciences*, https://doi.org/10.33063/diva-381852, 2019.

Zimmermann, N.E. and Kienast, F.: Predictive mapping of alpine grasslands in Switzerland: Species versus community approach. *Journal of Vegetation Science*, 10(4): 469-482, https://doi.org/10.2307/3237182, 1999.